DOI 10.1007/s11141-016-9721-7
Radiophysics and Quantum Electronics, Vol. 59, No. 7, December, 2016
(Russian Original Vol. 59, No. 7, July, 2016)

LONG-TERM GLOBAL DISTRIBUTIONS OF MESOSCALE VARIATIONS IN ATMOSPHERIC RADIO REFRACTION OBTAINED FROM THE GPS CHAMP SATELLITE DATA

N. M. Gavrilov* **and R. O. Manuilova**

UDC 537.876+551.51

We obtain average global distributions of the variances of the mesoscale variations in the atmospheric radio-refraction index (refractive index) at altitudes of 5–35 *km from the data of the radio-occultation experiments performed during operation of the low-orbit GPS CHAMP satellite in the period* 2001–2009. *The filtering of the vertical profiles of the radio-refraction index allows one to determine the variances of the variations with vertical scales below* 8 *km. The latitudinal-temporal distributions of the zonal-mean variances of the index demonstrate significant interannual variations at various altitudes. Seasonal variations in the variances of radio refraction are studied. Quasi-biennial oscillations at low latitudes are revealed. Acoustic-gravity waves and turbulent and convective motions in the atmosphere can cause a spread of the radio-refraction index.*

1. INTRODUCTION

The space-borne remote sensing using radio waves has been widely used in recent years for analyzing atmospheric processes, which allows one to obtain global information on the dynamic structures of the planetary scale and mesoscale disturbances of the atmospheric parameters. Intense experimental and theoretical studies, as well as the satellite data significantly improved our knowledge of variations in the refractive index under the action of atmospheric convection, waves, and turbulence.

Once developed, the global positioning system (GPS) has been used for studying the atmospheric parameters. The GPS satellites rotate round the Earth following the circular orbits at altitudes of about 20000 km, such that one rotation takes about 12 h and radio signals from these satellites are recorded by the receivers located on the ground surface or onboard low-orbit satellites. During the atmospheric propagation of centimeter radio waves, their trajectories are curved and propagation velocity is decreased. Measuring the phase variations of the radio signals received from several GPS satellites allows one to determine the receiver coordinates and vertical profiles of the atmospheric refractive index for radio waves.

The first experiments on the radio-occultation atmospheric sensing by radio signals from the GPS navigation system was conducted using a receiver mounted onboard the "Microlab-1" satellite in 1995–1997 [1, 2]. The limb phase measurements allowed us to obtain the vertical profiles of the refractive index of atmospheric air. In [3], it is shown that variations in the radio-signal phases are proportional to variations in the radio-refraction index $N_{\mathrm{r}} = (n-1)\cdot 10^6$, which was integrated along the radio beam (in this case, n is the refractive index). Comprehensive information on the mesoscale variations in the atmospheric parameters, which can be caused by both dynamic and wave processes [4–7], was obtained from the GPS "Microlab" data. The mesoscale-variation studies using the radio-occulation GPS experiments were continued from

* gavrilov@pobox.spbu.ru

St.Petersburg State University, St.Petersburg, Russia. Translated from Izvestiya Vysshikh Uchebnykh Zavedenii, Radiofizika, Vol. 59, No. 7, pp. 593–604, July 2016. Original article submitted June 16, 2015; accepted January 12, 2016.

the CHAMP satellite launched in April 2001 and then the COSMIC space-group satellites launched in 2006 [8–13].

In [6, 7], the relative variations $\delta N_{\rm r}/N_{\rm r}$ in the radio-refraction index according to the data of the GPS/MET satellite experiment are studied as the mesoscale-variability indicator for all atmospheric altitudes. Here, $\delta N_{\rm r}$ is the mesoscale-component variance obtained by filtering the vertical profiles $N_{\rm r}(z)$, which were measured from the GPS satellite. In this work, we study the distributions of the radio-refraction index variances with respect to altitude, latitude, and longitude using the data on refraction of the GPS radio signals recorded onboard the low-orbit satellite CHAMP in 2001–2009. The latitude–longitude structures of the mesoscale stratospheric variations are analyzed in [14–18] using the CHAMP-satellite measurements for shorter time intervals, which demonstrated significant irregularities of the mesoscale variances. Therefore, a large data volume is required to study the stable climatology features of the altitude-latitude distributions of the atmospheric mesoscale variances.

In this study, we analyzed over 250000 vertical profiles of the atmospheric radio-refraction index, which were measured by the CHAMP satellite during its operation period (2001–2009) and obtained from the database of the Center for Geophysical Studies in Potsdam, Germany. The latitude-altitude and latitude-longitude distributions of the variances of the mesoscale variations of the radio-refraction index in atmosphere, which were averaged over the above-mentioned period, are determined. Correlation of the mesoscale variability with the atmospheric stability is studied.

2. DATA ANALYSIS METHOD

In this work, we use the data of the 5th version of determining the atmospheric parameters from the CHAMP-satellite data [19]. Determination of the atmospheric parameters using the GPS-satellite database of the Center for Geophysical Studies in Potsdam, Germany started with correction of the satellite-watch differences using the method of double differences [20]. The refraction angles of radio beams for two frequencies were determined by the time differentiation of the redundant phase increment in the atmosphere after special filtering [21]. The ionospheric contribution was corrected with the help of a linear combination of the radio-beam refraction angles at two frequencies. To rule out the consequences of the multipath interference of radio waves at altitudes below 15 km, the method of full spectral inversion was used [22]. The vertical radio-refraction profiles in the atmosphere were determined from the corrected vertical profiles of the refraction angle, which were measured by the CHAMP satellite with an altitude step of 0.2 km. The methods employed to determine the atmospheric parameters are described in more detail in [22].

In the atmosphere, the refractive index $N_{\rm r}$ decreases with increasing altitude proportionally to the density decrease. Frequently, when analyzing the GPS-satellite data, the so-called "dry temperature" $T_{\rm dry} = Cp$ [mmHg]$/N_{\rm r}$, where p is the pressure and the constant $C = 77.6$ K/mBar, is introduced. The dry temperature ensures good estimation of the atmospheric temperature at altitudes exceeding 5–10 km. Since at the lower altitudes the refractive index can be influenced by humidity, the dry temperature can differ from that of the ambient air. Substantial errors because of the incomplete elimination of the ionospheric contribution [3] can arise at altitudes exceeding 5–10 km. The dynamic processes in the atmosphere cause variations in the pressure δp, temperature δT, and other parameters. The following relationship is usually fulfilled for the small-scale turbulence and low-frequency short acoustic-gravity waves: $|\delta p/p| \ll |\delta T/T|$ and it can be shown that $\delta T_{\rm dry}/T_{\rm dry} \approx \delta N_{\rm r}/N_{\rm r}$. In [6, 7], good feasibility of this relationship is shown using the GPS/MET-experiment data. Therefore, the relative deviation $\delta T_{\rm dry}/T_{\rm dry}$ can be used (along with $\delta N_{\rm r}/N_{\rm r}$) for estimating the refractive-index oscillations in the atmosphere.

In [3], it is shown that the study of the mesoscale variability of the atmospheric characteristics requires reduction of the vertical nonuniformity by filtering the large-scale components. For this purpose, various digital filters are used (see, e.g., [12, 13, 23, 24]). Numerical experiments show that after some parameter adjustment, different filter types yield almost equivalent results. In this study, we use the digital filters based on polynomial approximation [6, 7]. The smoothed values of the quantities $\ln N_{\rm r0}(z_i)$ or $T_0(z_i)$ are calculated for each altitude z_i of the satellite measurements using the least-square method approximation

of the corresponding vertical profiles $\ln N_{\rm r}(z)$ or $T_{\rm dry}(z)$ by the second-order polynomials inside the sliding altitude intervals with thickness Δz and the centers at the altitudes z_i. Then the mesoscale variations of the atmospheric radio-refraction index are estimated as the relative variances of deviations from these smoothed values: $\delta N_{\rm r}/N_{\rm r0}$ or $\delta T/T_0$. In this study, the layer thickness $\Delta z \approx 5$–10 km was used. The model calculations show that the above-described procedure is equivalent to the digital filter passing the spectral harmonics, which correspond to the vertical wavelengths $\lambda_z < 4$–8 km for $\Delta z \approx 5$–10 km, respectively.

For the above-described polynomial filtering, relatively thin layers with small Δz are used, no assumption of the vertical regularity is required, short computer time is involved, and a great number of the vertical profiles of the altitude-nonequidistant data can be processed. However, this filtering can overestimate the perturbation amplitudes near a very sharp tropopause [12, 13, 23, 24]. The studies in [13, 24] and the described numerical experiments show that the amplitude overestimations can occur only at distances below ±3–5 km from the tropopause and only if variations in the vertical gradient of the temperature in the tropopause region are sufficiently large. In the case of the discussed quadratic polynomial filtering, the altitude layers with the thickness $\Delta z \approx 5$–10 km are used. Therefore, the tropopause does not affect the results of the proposed analysis if the distance from the latter exceeds $\Delta z/2 \approx 3$–5 km. An additional precaution against the tropopause-induced artefacts is to exclude from the analysis the data for which the difference between the vertical temperature gradients in the upper and lower portions of the approximating layers exceeds 6 K/km. The values of the quadratic trend and the relative deviations from the latter are calculated for each node of the vertical profile of the refractive index measured by the CHAMP satellite. Then the variances of the above-mentioned deviations of the radio-refraction index are calculated for the specified altitudes, geographical regions, and various months of the entire interval of the CHAMP-satellite operation in 2001–2009.

In [25–27], it is shown that superposition of the radio rays arriving at the observation point from various trajectories becomes possible in the regions of the refraction-angle increase with increasing altitude. This can create false variations in the measured parameters, which are not related to the atmospheric processes. Such effects of the multipath propagation of radio waves is often observed in the lower atmosphere. The errors because of the multipath propagation of radio waves are estimated in [25] for the values of the atmospheric parameters obtained from the GPS-satellite data. The above-described analysis of the CHAMP data comprises complete spectral inversion [28], which reduces the influence of the multipath propagation of radio waves. However, significant profile peaks $N_{\rm r}(z)$, which can be interpreted as false perturbations of the atmospheric parameters, may remain in the regions of large irregularities of the refraction angles. To rule out such residual effects of the multipath propagation of radio waves, we disregarded all the data from the layers with a thickness of 1 km both above and below the levels in which we locally have $|{\rm d}\ln(N_{\rm r})/{\rm d}z - {\rm d}\ln(N_{\rm r0})/{\rm d}z| > 0.01$ km^{-1}. The statistical analysis of over 250000 profiles $N_{\rm r}(z)$, which were obtained from the CHAMP satellite, shows that such significant differences in the local and smoothed gradients was observed only in several percent of the cases and cannot influence the average mesoscale variances obtained in this study.

3. ANALYSIS RESULTS

Using the above-described methods, we processed the data of the radio-refraction index measurements from the GPS satellite CHAMP from April 2001 to April 2009. To analyze the altitude-latitude structure of the zonal-mean characteristics, we calculated the variances of the mesoscale variations in the refractive index, which were averaged over the entire 2001–2009 period of observations from the CHAMP satellite. Since comparing the results of using various vertical filters with the thicknesses $\Delta z = 5$ km and $\Delta z = 10$ km, we obtain almost the same distributions of the analyzed characteristics, in this work, we present the results only for $\Delta z = 10$ km.

The obtained mesoscale variances are shown in Fig. 1 for the data averaged over the winter (December–February, panel *a*) and summer (May–September, panel *b*) months for the Northern hemisphere for all the analyzed years. Figure 1 shows the existence of the principal maxima of the mesoscale variances of the

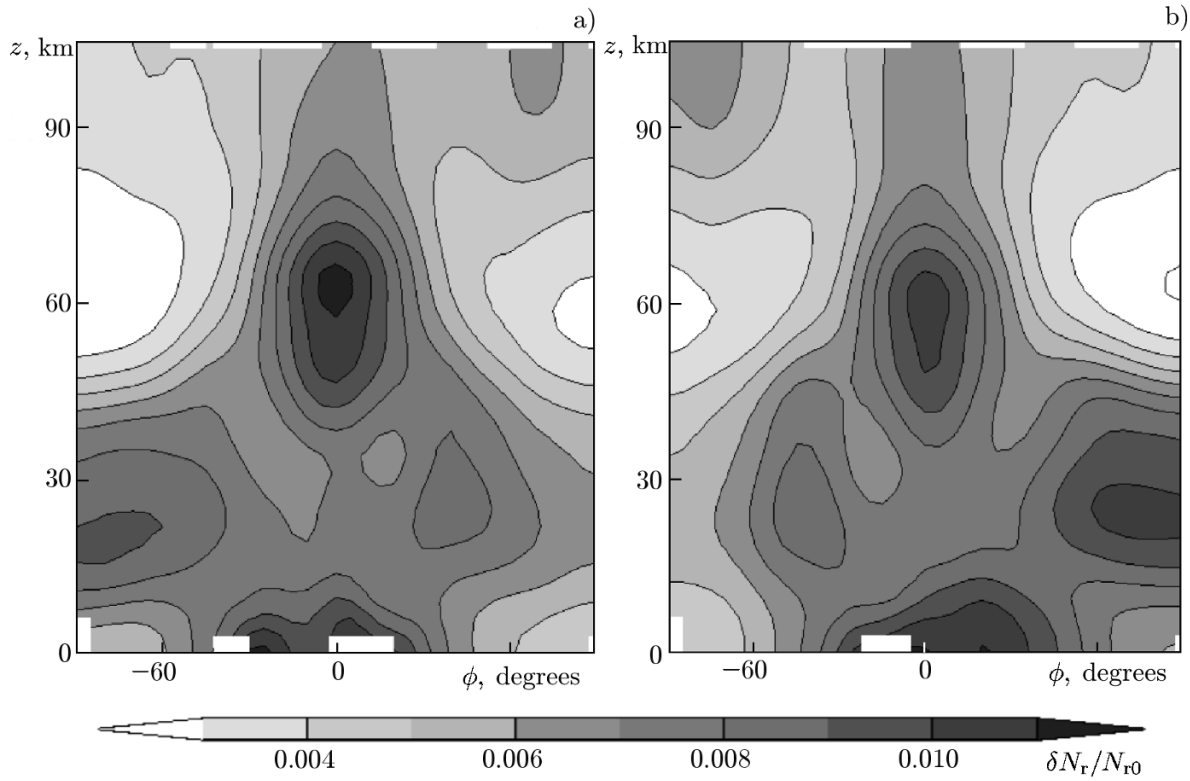

Fig. 1. The variance $\delta N_{\rm r}/N_{\rm r0}$ of the relative mesoscale perturbations of the radio-refraction index averaged over the longitude and time for the entire period of the radio-occulation measurements onboard the GPS satellite CHAMP in 2001–2009 for December–February (*a*) and May–September (*b*).

radio-refraction index at altitudes of 15–25 km in the equatorial latitudes, which can be related to the wave motions and tropical deep convection (see below). Figure 1 is also indicative of the increased variances at altitudes of 5–10 km, which correspond to the regions of the tropo-stratospheric jet streams (see illustrations in [8]), the regions above the tropopause, and can also be caused by other wave and turbulence sources in atmosphere. Comparing panels (*a*) and (*b*) in Fig. 1, one can follow the seasonal variations in the mesoscale variances, which are greater in the Southern hemisphere at altitudes of 5–15 km. At altitudes exceeding 20 km, the variances are greater in the winter season in the Northern and Southern hemispheres. This seems to reflect the seasonal variability of the sources of the mesoscale acoustic-gravity waves and background atmospheric fields influencing propagation of these waves. The distributions in Fig. 1 resemble similar distributions previously obtained from the data of the GPS/Microlab-1 experiment in 1995–1997 [6, 7] and the earlier information from the CHAMP satellite [17]. A similar distribution for the potential energy of the atmospheric acoustic-gravity waves above 5 km in December 2006 was obtained in [8] from the CHAMP-satellite data. This is indicative of good repeatability and stability of the altitude-latitude zonal-mean mesoscale distributions of the radio-refraction index in various satellite experiments in various years. Such stable results can prove that the distributions presented in Fig. 1 are not related to random measurement errors, but reflect actual variations in the atmospheric parameters.

Figures 2 and 3 show the latitude-longitude distributions of the mesoscale variances of the atmospheric radio-refraction index in various altitude layers for the winter and summer months of the Northern hemisphere, respectively. Since humidity at altitudes of 15–30 km is low, the radio-refraction variances reflect the temperature and atmospheric-density variability. At the lower altitudes, an additional variability can result from the water-vapor density variations.

The refractive-index variations can be caused by the dynamic processes which create irregularities in the atmospheric-parameter distribution. Therefore, the variations presented in Figs. 2 and 3 can show

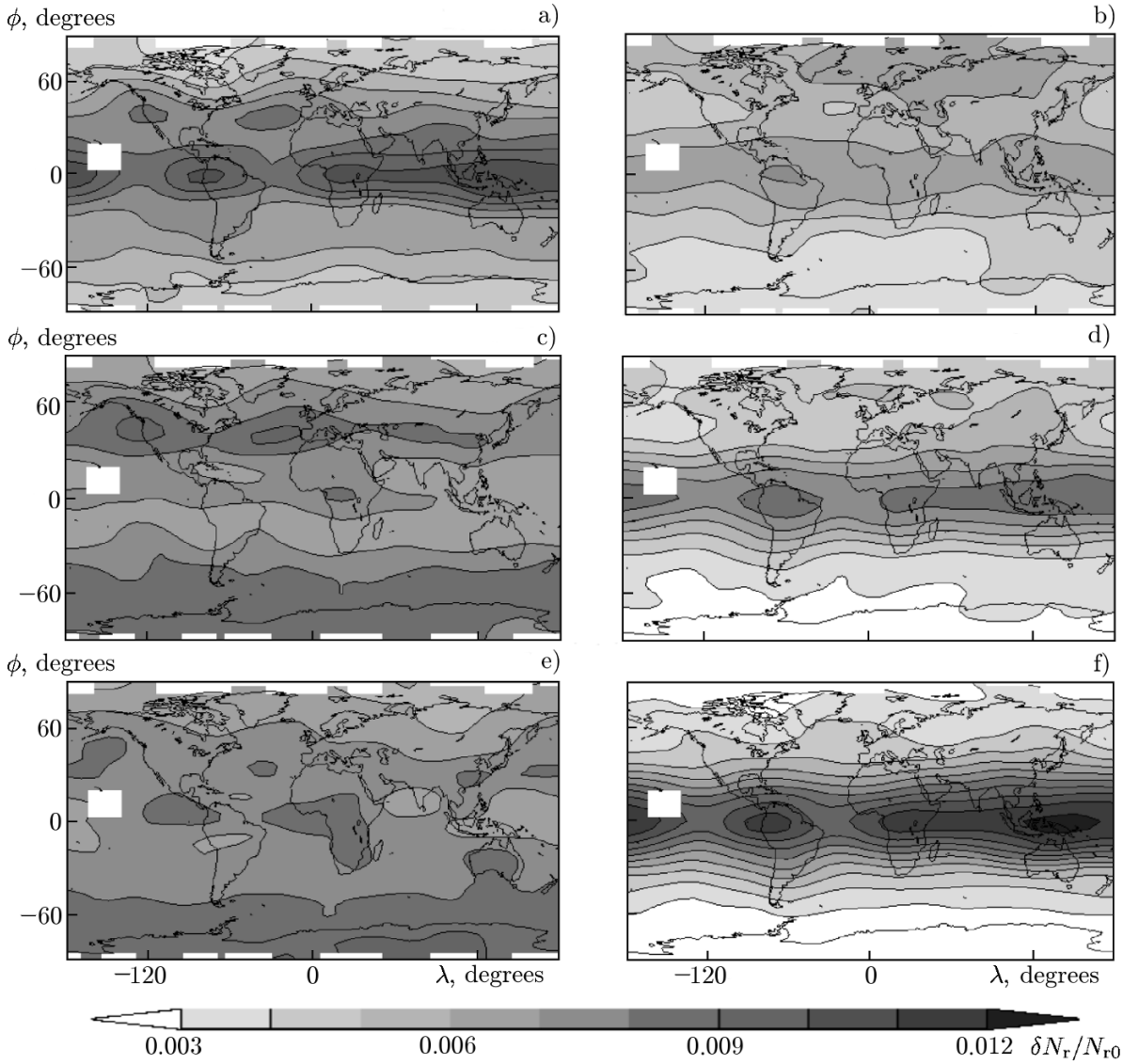

Fig. 2. The latitude-longitude distributions of the variances of the relative mesoscale radio-refraction perturbations for December–February, which are averaged over the period 2001–2009 using the data from the GPS CHAMP satellite at the altitudes $z = 15$ km (*a*), 30 km (*b*), 10 km (*c*), 25 km (*d*), 5 km (*e*), and 20 km (*f*).

the distributions of the intensities of the meso- and small-scale dynamic variations in the fixed altitude layers. These variations can be caused by the mesometeorological and convective processes, as well as the atmospheric acoustic-gravity waves and turbulence. In the troposphere, the amplitudes of these waves are usually small and a mesoscale turbulence can considerably contribute to the radio-refraction index variations. The wave amplitudes increase with increasing altitude and their contribution to the mesoscale variability of the refractive index becomes greater.

As is obvious from Fig. 2, in the midlatitudes and at altitudes below 10 km, the radio-refraction variances averaged over December–February 2001–2009 have maxima, which can reflect convective activity. At altitudes of about 10 km, these maximum values correlate with the location of the tropospheric jet streams, which have the intensity maxima at altitudes of 10–12 km (see the illustration in [8]). At altitudes from 15 to 25 km and latitudes from 20° S to 20° N, the maxima in Fig. 2 can be related to the convective and wave processes in the equatorial region (see below). Figure 3 shows the same as Fig. 2, but for the period from May to September. The main difference between Figs. 2 and 3 is in the seasonal variations at

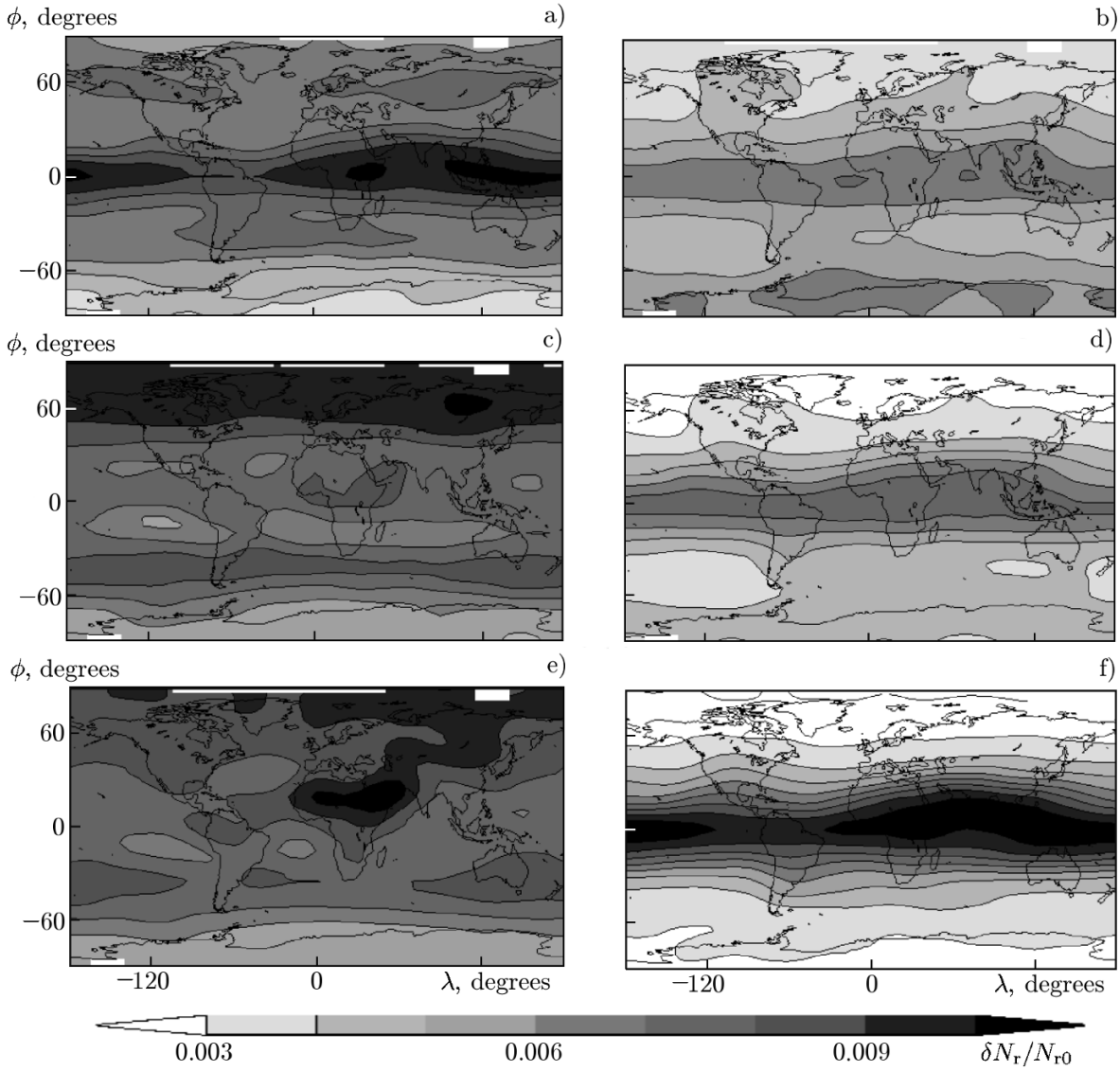

Fig. 3. The same as in Fig. 2, but for May–September 2001–2009.

altitudes exceeding 20 km, where the variances of the mesoscale variability are greater in the winter seasons in each hemisphere.

The above-mentioned seasonal fluctuations are more pronounced in Fig. 4 in which the time variations of the zonal-mean variances for various latitudes and altitude layers are shown. Figure 4 shows the annual variations of the variances of the atmospheric radio-refraction index for the middle and high latitudes. Below 15 km, the variances are maximum at latitudes exceeding 40°–50° in the Northern and Southern hemispheres in the summer seasons corresponding to these hemispheres. As is obvious from Fig. 4, the maximum variances in the stratosphere at altitudes of 25–30 km are observed in the winter seasons in each hemisphere. For the equatorial region above 15 km, Fig. 4 demonstrates a quasi-biennial oscillation with the variance maxima in the winter seasons of 2002, 2004, 2006, and 2008.

The small- and mesoscale motions depend on the Brunt–Väisälä frequency, which determines stability of the vertical profiles of the temperature in the atmosphere. To ensure a better interpretation of the above-described observed distributions of the mesoscale variances of the atmospheric radio-refraction index, the smoothed values of the temperature $T_0(z)$ (see Sec. 3) were used and the Brunt–Väisälä frequency squares $N^2 = g(\mathrm{d}T_0/\mathrm{d}z + \gamma_a)/T_0$, where γ_a is the dry adiabatic temperature gradient, were calculated. The N^2

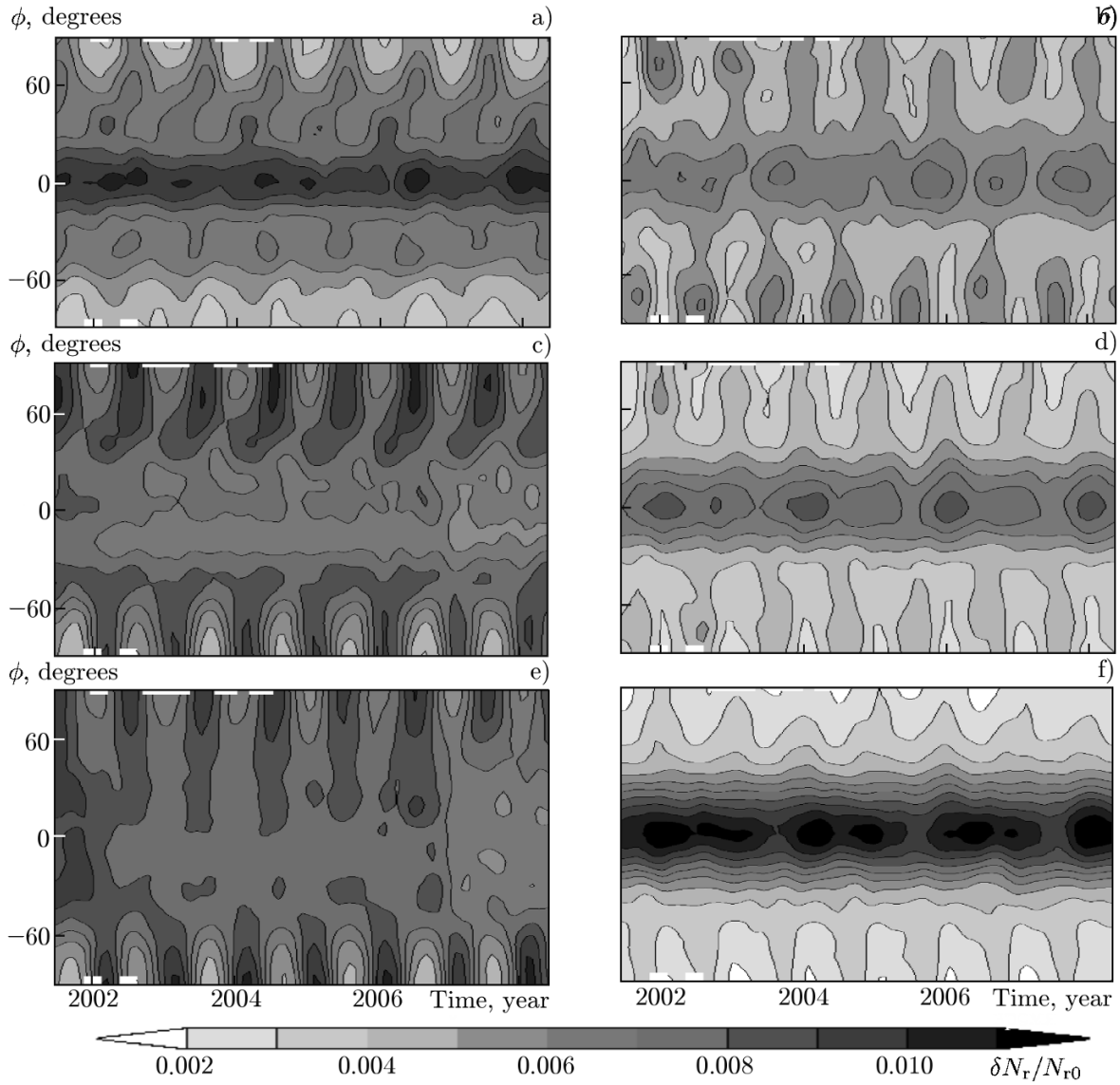

Fig. 4. The latitude-temporal variations of the zonal-mean relative variances of the mesoscale radio-refraction variations at the altitudes $z = 15$ km (*a*), 30 km (*b*), 10 km (*c*), 25 km (*d*), 5 km (*e*), and 20 km (*f*).

variations are shown in Fig. 5.

Comparing Figs. 4 and 5, one can see the presence of positive correlations between the variances of the mesoscale variations of the radio-refraction index and the Brunt–Väisälä frequency at altitudes of 5–15 km. At the tropospheric middle and high latitudes in both hemispheres, the quantity N^2 has its maxima in the appropriate summer seasons (see Fig. 5), which correspond to the mesoscale-variance maxima in Fig. 4. In stratosphere above 20 km, these N^2 maxima are shifted to the winter seasons in each hemisphere by analogy with the corresponding variance maxima in Fig. 4. In Fig. 5, in the equatorial region at altitudes of about 20 km, one can see quasi-biennial oscillations of N^2 with the local maxima in the winter seasons of 2002, 2004, 2006, and 2008. These maxima are in good agreement with those of the quasi-biennial oscillations of the radio-refraction variances in Fig. 4.

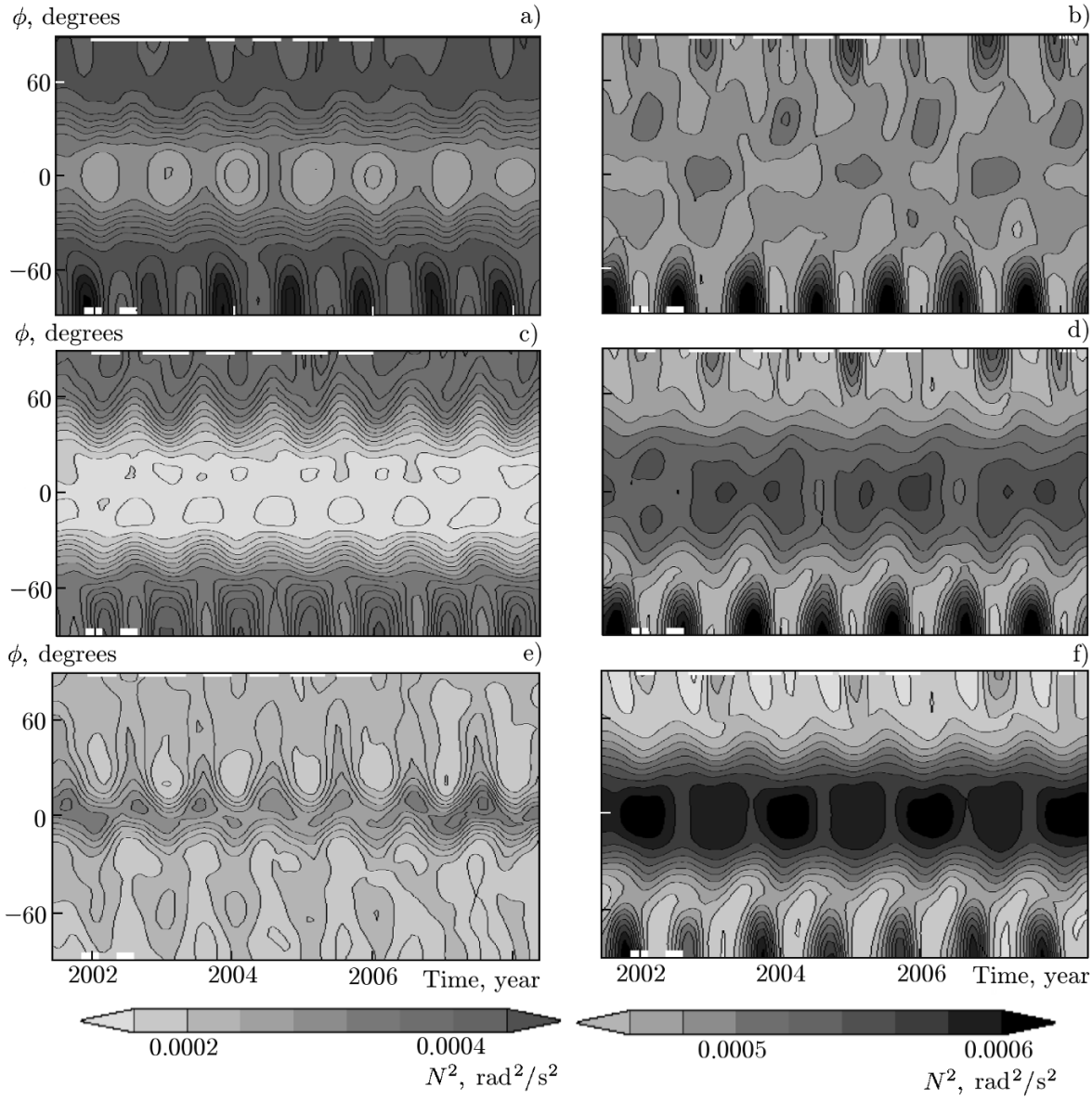

Fig. 5. The latitude-time variations of the squared Brunt–Väisälä frequency N^2 at altitudes $z = 15$ km (*a*), 30 km (*b*), 10 km (*c*), 25 km (*d*), 5 km (*e*), and 20 km (*f*).

4. DISCUSSION

In [12], the data of the COSMIC satellite system for the period from December 2006 to February 2007 were used, and the parameters of the acoustic-gravity waves at altitudes of 17–23 km were estimated. The latitude-longitude distributions of the temperature oscillations under the action of the acoustic-gravity waves, which resemble those represented in Fig. 2 for altitudes of 20–25 km, were obtained. The distributions obtained in [12] are more variable because of the shorter observation interval, but have the same maxima above South America, Africa, and the Pacific, as well as the distributions in Fig. 2 at an altitude of 20 km. Similar regions of the increased mesoscale variability in the equatorial region were observed in [9]. The above-mentioned studies used totally different methods for filtering artificial perturbations caused by the tropopause (see Sec. 3), which are based on analyzing the horizontal structure of the background temperature and using various digital filters. Therefore, similarity of their results with those given in Fig. 2 can testify to the fact that the observed maxima of the mesoscale radio-refraction variability at altitudes of 20–25 km

are not artefacts of the tropopause approximation or the method of the data filtering but reflect the actual mesoscale variability which exists in the middle atmosphere.

The theory of acoustic-gravity waves and atmospheric turbulence relates the temperature-variation variances $|\delta T/T|$ and the horizontal velocity $|\delta V|$ in the form $|\delta T/T| = N|\delta V|/g$. Thus, for equal $|\delta V|$, the relative temperature variations should be greater in the regions with a greater Brunt–Väisälä frequency. In addition, the mesoscale atmospheric gravity waves are vertically propagating at the frequencies $\omega < N$ and trapped at $\omega > N$. Therefore, an increase in the frequency N leads to the broadening of the frequency spectrum of the gravity waves propagating in the atmosphere. Both effects can stipulate contribution to the positive correlation between the variances of the mesoscale variations in the radio-refraction index and N^2, which is observed in Figs. 4 and 5.

The principal maxima of the mesoscale variances of the radio-refraction index in Fig. 1 are observed at altitudes of about 20 km near the equator. Similar maxima for the potential energy $E_\mathrm{p} = |\delta T/T|^2 g^2/(2N^2)$ of the acoustic-gravity waves were recorded in these regions according to the data from the CHAMP [16] and COSMIC [8] satellites, such that an increase in the amplitudes of not only the temperature variations, but also the velocity perturbations was observed. This can be due to an increase in the Brunt–Väisälä frequency above the tropopause. Numerical simulation and the experiments using the Japanese MCT radar [29] show that a sharp increase in the Brunt–Väisälä frequency can lead to an appropriate increase in the amplitudes of the atmospheric acoustic-gravity waves propagating from below. Estimated tropopause altitudes of 15–17 km near equator [8] show that the regions of the increased mesoscale perturbations of the radio-refraction index are located several kilometers above the tropopause. For such tropopause altitudes, during the numerical simulation [29] of propagation of the acoustic-gravity waves, it was found that their amplitudes are maximal at altitudes of about 20 km, which is in good agreement with the equatorial-maximum location in Fig. 1. These numerical experiments show that a sharp increase in the acoustic-gravity waves above the tropopause can lead to their instability and generation of the small-scale turbulence, which can also contribute to the observed variability of the atmospheric parameters.

The potential energy of the acoustic-gravity waves at altitudes of 15–35 km was studied in [16] using the CHAMP data for 2001–2006. The biennial oscillations with the potential-energy maxima in 2002, 2004, and 2006, which are similar to those represented in Fig. 4, were observed. The seasonal oscillations of potential energy with the winter maxima in both hemispheres, which are identical to those in Fig. 4 at an altitude of 40 km, are found in [16] at altitudes of 30–35 km. Since the potential energy reflects intensity of the acoustic-gravity waves, the above-mentioned features of the radio-refraction index variations in Fig. 4 above 15 km can be explained by variations in the wave sources and the conditions of propagation of the mesoscale waves in various years and seasons in the middle atmosphere.

The vertical momentum fluxes produced by long inertial-gravity waves are estimated in [12]. These fluxes have maxima above the equatorial South America, Africa, and Scandinavia (where the local maxima of the radio-refraction variances are located at an altitude of 25 km, see Fig. 2). Therefore, the regions with increased radio-refraction perturbation can be considered as the sources of the acoustic-gravity waves propagating in the middle atmosphere.

The orography distribution along the equator was studied in [17], and it was revealed that the maxima of the mesoscale variances of radio refraction in Fig. 2 at altitudes of 20–25 km are located above the mountain areas of South America and South-East Asia. The most and the least extended mountain systems are located in Africa and South-East Asia, respectively. In [9], the outgoing longwave radiation is used as an indicator of the presence of deep convection in the equatorial zone. Three maxima coinciding with the radio-refraction variance maxima, which are shown in Fig. 4 at altitudes of 20–25 km, were observed in December–February 2007. Therefore, the internal mesoscale acoustic-gravity waves propagating in the middle atmosphere from orographic and convective sources and the wave enhancement above the tropopause due to a sharp increase in the Brunt–Väisälä frequency can create the stable maxima of the mesoscale radio-refraction variability at altitudes of 20–25 km above the equator.

The mesoscale temperature variations measured by the microwave limb sounder (MLS) from the Aura

satellite during the period 2005–2008 are analyzed in [30]. In [30], Fig. 9 resembles Fig. 4 in this work. It also shows maximum mesoscale temperature variations at altitudes of 20–30 km in the winter periods in both hemispheres. Analyzing Fig. 9 in [30], we see consistency of the structure of the seasonal oscillations at altitudes of up to 45 km.

In [30, 8], good correspondence between the variances of the mesoscale temperature perturbations and the structure of the stratospheric zonal jet streams is found. Using the Sec. 2 results, one can conclude that variations in the jet streams and the Brunt–Väisälä frequency can influence the temporal, latitudinal, and longitudinal structures of the mesoscale variances of the atmospheric refractive index.

5. CONCLUSIONS

In this work, we have analyzed the mesoscale variations of the refractive index (dry temperature) in the atmosphere at altitudes of 5 to 35 km, which were obtained from the data of the eight-year GPS/CHAMP satellite experiment. The radio-refraction variations can yield information on the global distribution of the dynamically active zones in the atmosphere in which the turbulence enhancement and generation of the acoustic-gravity waves can be expected. Variations in the jet streams and the Brunt–Väisälä frequency can influence the temporal and spatial structures of the mesoscale variances of the atmospheric temperature and refractive index. The zonal-mean mesoscale variances of the atmospheric radio-refractive index have maxima at altitudes of 15 to 25 km and latitudes from 20° S to 20° N, which can be related to generation and propagation of the acoustic-gravity waves in the equatorial atmosphere. At altitudes of about 10 km, the maxima of the mesoscale radio-refraction variances correlate with the jet-stream location in the upper troposphere. Above 25 km, the radio-refraction index variances are greater in winter than in summer in both hemispheres. There exists positive correlation between the mesoscale variances of the refractive index and the Brunt–Väisälä frequency in the stratosphere.

We thank J. Wickert and Ch. Reigber for kindly providing the data from the GPS CHAMP satellite and A. N. Gavrilov for assistance in the software development. The study was financially supported by the Russian Foundation for Basic Research (project No. 13-05-00443A).

REFERENCES

1. R. Ware, C. Rocken, F. Solheim, et al., *Bull. Amer. Meteorol. Soc.*, **77**, No. 1, 19 (1996).
2. C. Rocken, R. Athes, M. Exner, et al., *J. Geophys. Res.*, **102**, No. D25, 29849 (1997).
3. A. S. Gurvich, V. Kan, and O. V. Fedorova, *Izv. Atmos. Oceanic Phys.*, **36**, No. 3, 300 (2000).
4. T. Tsuda, M. Nishida, C. Rocken, et al., *J. Geophys. Res.*, **105**, No. D6, 7257 (2000).
5. M. J. Alexander, T. Tsuda, and R. A. Vincent, *J. Atmos. Sci.*, **59**, No. 8, 1394 (2002).
6. N. M. Gavrilov, N. V. Karpova, Ch. Jacobi, et al., *J. Atmos. Solar-Terr. Phys.*, **66**, No. 6, 427 (2004).
7. N. M. Gavrilov and N. V. Karpova, *Izv. Atmos. Oceanic Phys.*, **40**, No. 6, 668 (2004).
8. S. P. Alexander, T. Tsuda, and Y. Kawatani, *Geophys. Res. Lett.*, **35**, No. 10, L10808 (2008).
9. S. P. Alexander, T. Tsuda, Y. Kawatani, et al., *J. Geophys. Res.*, **113**, No. 24, D24115 (2008).
10. P. Alexander, D. Luna, A. de la Torre, et al., *Adv. Space Res.*, **45**, No. 10, 1231 (2010).
11. L. Wang and M. J. Alexander, *J. Geophys. Res.*, **114**, No. D18, D18108 (2009).
12. L. Wang and M. J. Alexander, *J. Geophys. Res.*, **115**, No. D21, D21122 (2010).
13. T. Schmidt, A. de la Torre, and J. Wickert, *Geophys. Res. Lett.*, **35**, No. 16, L16807 (2008).
14. M. Venkat Ratnam, G. Tetzlaff, and Ch. Jacobi, *J. Atmos. Sci.*, **61**, No. 13, 1610 (2004).

15. A. de la Torre, T. Tsuda, G. A. Hajj, et al., *J. Meteorol. Soc. Japan*, **82**, No. 1B, 407 (2004).
16. A. de la Torre, T. Schmidt, and J. Wickert, *Geophys. Res. Lett.*, **33**, No. 24, L24809 (2006).
17. N. M. Gavrilov, *Izv. Atmos. Oceanic Phys.*, **43**, No. 4, 451 (2007).
18. S. P. Namboothiri, J. H. Jiang, P. Kishore, et al., *J. Geophys. Res.*, **113**, No. 7, D07102 (2008).
19. J. Wickert, G. Beyerle, R. K´onig, et al., *Ann. Geophys.*, **23**, No. 3, 653 (2005).
20. J. Wickert, R. Galas, T. Schmidt, et al., *Phys. Chem. Earth.*, **29**, No. A2-3, 267 (2004).
21. W. H. Press, S. A. Teukolsky, W. T. Vetterling, et al., *Numerical Recipes in FORTRAN 77. The Art of Scientific Computing*, Cambridge University Press, Cambridge (1996).
22. J. Wickert, T. Schmidt, G. Beyrle, et al., *J. Meteorol. Soc. Jap.*, **82**, No. 18, 381 (2004).
23. T. Horinouchi and T. Tsuda, *J. Geophys. Res.*, **114**, No. D16, D16110 (2009).
24. P. Alexander, A. de la Torre, P. Llamedo, et al., *Atmos. Meas. Tech. Disc.*, **4**, No. 1, 1181 (2011).
25. M. E. Gorbunov, K. B. Lauritsen, A. Rodin, et al., *Izv. Atmos. Oceanic Phys.*, **41**, No. 6, 726 (2005).
26. M. E. Gorbunov and A. S. Gurvich, *J. Geophys. Res.*, **103**, No. D12, 13819 (1998).
27. M. E. Gorbunov, A. S. Gurvich, and L. Korblueh, *Radio Sci.*, **35**, No. 4, 1025 (2000).
28. A. S. Jensen, M. Lohmann, H. H. Benzon, et al., *Radio Sci.*, **38**, No. 3, 1040 (2003).
29. N. M. Gavrilov and S. Fukao, *Ann. Geophys.*, **22**, No. 11, 3889 (2004).
30. D. L. Wu and S. D. Eckermann, *J. Atmos. Sci.*, **65**, No. 12, 3695 (2008).